5 CHANGE IN TETRACENE POLYMORPHISM FACILITATES TRIPLET TRANSFER IN SINGLET FISSION-SENSITIZED SILICON SOLAR CELLS

This chapter is based on the following publication [20]:

Benjamin Daiber*, Sourav Maiti*, Silvia M Ferro, Joris Bodin,Alyssa FJ van den Boom, Stefan L Luxembourg, Sachin Kinge, Sidharam P Pujari,Han Zuilhof, Laurens DA Siebbeles, and Bruno Ehrler. "Change in Tetracene Polymorphism Facilitates Triplet Transfer in Singlet Fission-Sensitized Silicon Solar Cells" In: *The Journal of Physical Chemistry Letters* (2020)

Singlet fission in tetracene generates two triplet excitons per absorbed photon. If these triplet excitons can be effectively transferred into silicon (Si) then additional photocurrent can be generated from photons above the bandgap of Si. This could alleviate the thermalization loss and increase the efficiency of conventional Si solar cells. Here we show that a change in the polymorphism of tetracene deposited on Si due to air exposure, facilitates triplet transfer from tetracene into Si. Magnetic field-dependent photocurrent measurements confirm that triplet excitons contribute to the photocurrent. The decay of tetracene delayed photoluminescence was used to determine a transfer efficiency into Si of around 36 %. Our study suggests that control over the morphology of tetracene during the deposition will be of great importance to boost the triplet transfer yield further.

5.1 INTRODUCTION

Silicon is currently the dominating semiconductor material for solar cells, but suffers from several loss mechanisms that reduce its efficiency [103, 108]. The largest loss mechanism results from the inefficient utilization of high-energy photons. The additional energy between the Si band gap and the high-energy photons is lost to heat. Sensitizing Si solar cells with a top layer of singlet fission material can reduce this loss, and theoretically even overcome the detailed balance efficiency limit of ~ 31 % for a single-junction solar cell [7, 17, 30, 34, 37, 64, 84, 91, 104, 115, 119, 128].

Singlet fission is a spin-allowed process of creating two triplet excitons from one singlet exciton that can occur in certain organic semiconductor materials with delocalized π-orbitals [117–119, 124]. In this paper, we will focus on tetracene, which consists of four benzene rings that are annularly and linearly fused (Figure 5.1). Upon absorption of a high-energy photon ($> 2.4\,\mathrm{eV}$), a singlet exciton (bound electron-hole pair) is formed. This singlet exciton (S_1) can subsequently be split into two triplet excitons (T_1) with each roughly half the energy of the singlet exciton. This singlet fission process is mediated by a pair of spin-correlated triplets (TT), based on the kinetic model proposed by Johnson and Merrifield in 1970 [44, 56]:

$$S_0 + h\nu \Rightarrow S_1 \Rightarrow (TT) \Rightarrow T_1 + T_1$$

where S_0 is the singlet ground state, $h\nu$ the incoming photon energy, and $T_1 + T_1$ a pair of free triplets. In this model, the rate of singlet fission is determined by the coupling between the S_1 and TT states [80, 94]. Singlet fission competes with other processes (e.g. radiative and non-radiative recombination and excimer formation), such that some singlet excitons are lost and cannot undergo singlet fission. In tetracene, one absorbed photon leads to close to 2 triplet excitons, as singlet fission is very fast compared to other competing decay channels [11, 13].

In a solar cell architecture where the triplet exciton is transferred into Si, the bandgap of the Si cell has to be smaller than the energy of the triplet

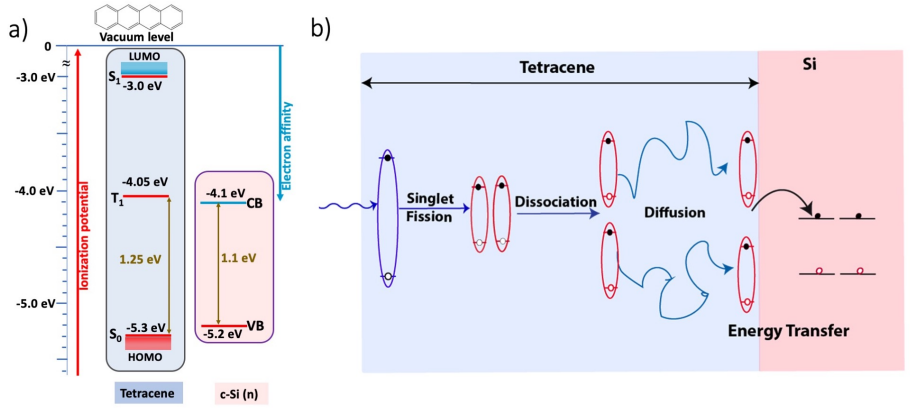

Figure 5.1: a) Energy alignment of tetracene in the ground state (S_0), triplet state (T_1), singlet state (S_1) and Si valence band (VB) and conduction band (CB) from the literature [13, 76, 131, 149]. The structure of tetracene is shown at the top. b) Schematic of a singlet fission-sensitized Si solar cell. Photons at or above the singlet energy of tetracene are absorbed and create one singlet exciton, which splits into two triplet excitons forming a correlated triplet pair (TT) via singlet fission. The TT dissociates into free triplets which can then independently diffuse to the tetracene-Si interface and transfer into Si to generate free charge carriers.

exciton state of the singlet fission material. In tetracene, the triplet energy is $\sim$ 1.25 eV which exceeds the Si bandgap of 1.1 eV, allowing triplet exciton transfer [13, 76, 109, 131]. The V_{oc} is determined by the low-bandgap semiconductor Si and the photocurrent from the high-energy photons can be doubled due to singlet fission that eventually generates two electron-hole pairs from the high-energy photons of energy > 2.4 eV.

Triplet transfer to Si can happen through energy transfer or charge transfer. In the case of energy transfer, both electrons and holes arrive in Si concurrently. However, if either electrons or holes are transferred into Si via charge transfer, the remaining countercharges in tetracene have to be extracted by an additional contact [76]. Hence, if triplet energy transfer into Si could be realized the resulting tetracene-Si solar cell would not need an additional charge extracting electrode on top of the tetracene

layer. Therefore, energy transfer could in principle enable a simpler solar cell architecture and less added cost to silicon solar cell manufacturing. As the tetracene triplet energy is higher than the Si band gap, transfer into Si is energetically allowed. Figure 5.1 a) shows the ionization energy of the tetracene exciton states and the position of the Si bands. The absolute energy level of the triplet exciton ionization energy with respect to the vacuum level is reported to be in the range of −4.0 eV to −4.3 eV [13, 76]. Figure 5.1 b) shows a schematic of the processes involved in the operation of a singlet fission-sensitized Si solar cell, singlet generation, singlet fission, triplet diffusion, and triplet transfer.

To date, the transfer of triplet excitons from the singlet fission layer to the underlying low-bandgap semiconductor has proven to be the bottleneck for real-world applications. The extraction of triplets directly from tetracene into Si has been investigated by several research groups. Piland et al. did not find any evidence of triplet transfer from tetracene into Si upon direct deposition and with a LiF spacer [95]. MacQueen et al. reported a small contribution of triplets to the photocurrent upon direct deposition of tetracene on a Si solar cell [76]. The reasons for inefficient triplet transfer could be related to insufficient passivation of the Si surface and the weak coupling between the triplet exciton molecular orbitals and the electronic states in Si. Recently, Einzinger et al. unambiguously reported successful triplet transfer from tetracene into Si with 75% efficiency after passivating the Si with a thin (8 Å) dielectric layer of hafnium oxynitride (HfO_xN_y)grown through atomic layer deposition (ALD) [29]. The ALD-grown interlayer passivates the Si surface and is thin enough to allow the transfer of triplets from tetracene into Si. However, this system is very sensitive to the exact interlayer thickness and composition, and the effect of the tetracene structure remains unclear. The transfer mechanism is still under debate and additional self-passivation effects complicate the interpretation.

Here we report evidence for the triplet exciton transfer in a simpler system, from tetracene into bare Si, after exposure of the tetracene layer to ambient air. We find signatures of triplet exciton transfer in magnetic field-dependent photocurrent measurements and a faster decay of the delayed photoluminescence (PL) from tetracene, indicating triplet exciton

quenching. We correlate these changes to a change in tetracene morphology as seen in X-ray diffraction (XRD) spectra that show the conversion of polycrystalline tetracene from polymorph I (TCI) to polymorph II (TCII) [5, 112]. We propose that the change of tetracene polymorph is important for the observed triplet transfer into Si solar cells.

5.2 RESULTS

5.2.1 Triplet Signature in Photocurrent

Measuring the effect of triplet excitons on the photocurrent of a solar cell is the most direct way of measuring the transfer of triplet excitons, and is most relevant for the real-world application of a singlet fission-sensitized Si solar cell. The final goal is to increase the Si photocurrent from transferred triplet excitons. However, both singlet and triplet excitons can contribute to the photocurrent. Therefore, it is important to prove whether photocurrent originates from triplet versus singlet excitons. To distinguish between singlet and triplet exciton transfer we exploit the behavior of singlet fission under a magnetic field (see Figure 5.2). Under a magnetic field of 300 mT singlet fission in tetracene becomes less efficient, resulting in a lower triplet exciton population compared to the situation without the magnetic field [79]. The characteristic shape of the photocurrent change under a magnetic field can be unambiguously attributed to triplet excitons originating from singlet fission [29, 44, 144]. If the photocurrent from Si has the same magnetic field dependence as the triplet population (blue curve in Figure 5.2 a)) we conclude that there is transfer of triplet excitons into Si.

The photocurrent is caused prevalently by triplet transfer; the opposite magnetic field dependence (yellow curve in Figure 5.2 a) would indicate that the photocurrent is dominated by singlet transfer or radiative transfer. The relationship between magnetic field and singlet fission efficiency (or singlet/triplet populations) is not monotonic, below 50 mT there is a small dip in the opposite direction as described by Merrifield et al. (see also Figure 5.2 a) [79]. This characteristic curve also allows us to exclude

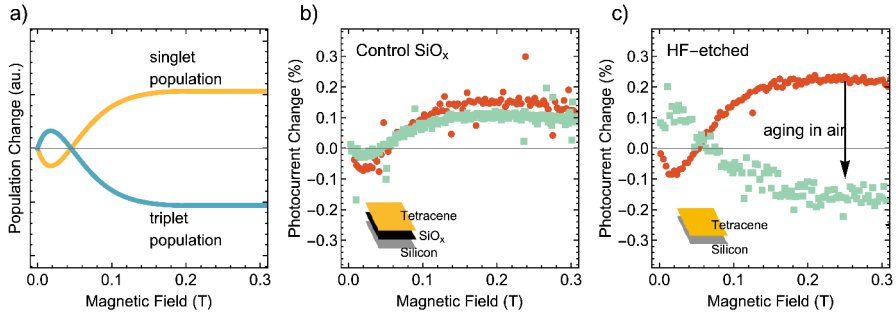

Figure 5.2: a) Schematic for the behavior of singlet and triplet population in tetracene for photocurrent as a function of the magnetic field. b/c) Magnetic field-dependent photocurrent measurements for b) Si/SiO_x/tetracene (control), and c) HF-Si/tetracene, both before (red curve) and after (green curve) exposure to air. For both samples b) and c) the positive change in photocurrent can be attributed to the dominant contribution of singlets. Aging the HF-etched sample in air flips the curve and leads to a triplet curve, indicating that triplets are transferred and contributing to the Si photocurrent.

any other effects that the magnetic field could have on the photocurrent, like a displacement of the sample, induced currents at the contacts, or sample degradation over time.

We fabricated Si solar cells with an additional tetracene singlet fission top layer. The solar cells are heterostructure with intrinsic thin (HIT) layer solar cells with an interdigitated back contact (IBC). This means that contacts are on the back, which allows free access to the front surface. The solar cells are then encapsulated in an inert N_2 atmosphere between two glass slides to keep oxygen and moisture out. Between the tetracene layer and the Si solar cell we used different interlayers for reference measurements and to gain insight into the transfer mechanism. We then measured the photocurrent as a function of an externally applied magnetic field as described above. Figure 5.2 b) shows the magnetic field dependent photocurrent of solar cells with an insulating interlayer of $\sim 2\,\text{nm}$ SiO_x, which shows no signature of triplet exciton transfer. A thick ($\sim 80\,\text{nm}$) Si_3N_4 (SiN) interlayer shows the same blocking behavior, as

shown in Figure 5.6 a) in the Appendix. The photocurrent follows the curve we would expect for singlet excitons, indicating that the singlet excitons contribute to the photocurrent. Utilizing a HF-etch to remove the blocking layer and enabling direct contact between tetracene and Si (HF-Si/tetracene) does not change this behavior, as seen in Figure 5.2 c) (red curve), which is in line with earlier reports [95]. The photocurrent still follows the singlet exciton population, and no evidence for triplet transfer is observed.

Si/SiO_x/tetracene and HF-Si/tetracene samples were then stored in the air under ambient conditions in the lab for five days and re-measured (Figure 5.2 b) and c)). The magnetic-field dependence of the photocurrent curve for the HF-Si/tetracene solar cell, shown in Figure 5.2 c), reverses for the air-exposed sample, closely following the characteristic shape for a triplet exciton population, which is strong evidence for triplet exciton transfer. If we encapsulate the solar cell and store it in air, we also observe the triplet curve, although its emergence is then much slower, i.e. after six weeks, as shown in Figure 5.6 b) (see Appendix), indicating that eventually, air enters the encapsulation. If the HF-Si/tetracene solar cell is stored under a dry nitrogen atmosphere in the glovebox ($< 10\,\mathrm{ppm}\,O_2; < 1\,\mathrm{ppm}\,H_2O$), we instead observed the singlet curve, which was retained after six weeks (Figure 5.6 c), Appendix). The strong difference in magnetic-field photocurrent behavior between the air-exposed and nitrogen-stored samples indicates that air-exposure plays a crucial role in enabling successful triplet transfer to Si. In Figure 5.2 c) the decrease in photocurrent at high field is around 0.2%, which is comparable to silicon-tetracene solar cells with HfO_xN_y interlayers [29]. In that study the self-passivation in Si, due to improved surface screening by charge carriers at the Si interface, caused an increased photocurrent [29]. This self-passivation can lead to an overestimation of the contribution of triplet exciton injection, and the effects of triplet excitons and self-passivation were separated by a strong background illumination. We performed similar experiments to investigate the self-passivation of Si in our samples by using a strong (100 W) xenon light source with red light below the absorption onset of tetracene but above the absorption onset of Si. This allows us to inject charge carriers directly in Si that

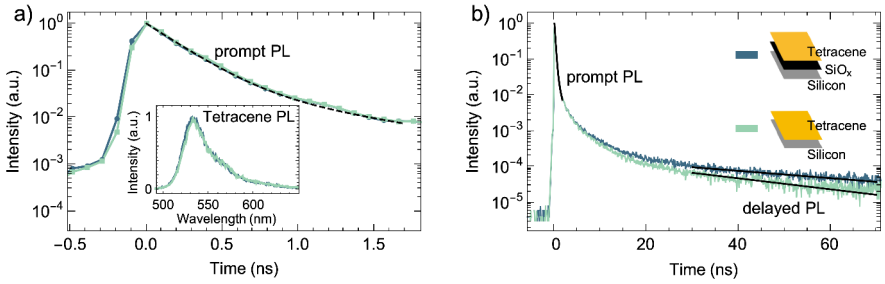

Figure 5.3: The PL decay traces in Si/SiO_x/tetracene and HF-Si/tetracene solar cells. Both samples have been aged in the air under similar conditions. The dotted black line represents the output from the kinetic model; a) short-time (prompt) PL shows no difference in singlet fission time and efficiency between samples; b) long time (delayed) PL shows faster decay for the HF-Si/tetracene solar cell, which we attribute to triplet transfer into Si. The inset in a) shows the PL spectra of both samples.

cannot have originated in tetracene. We did not see an influence of this additional light on the photocurrent change under the magnetic field after correcting for the additional bias current, so we can exclude large influences from self-passivation in the Si solar cell (see Figure 5.7, Appendix). Therefore, we can conclude that exposure to air leads to triplet transfer from tetracene into Si. We also measured the external quantum efficiency (EQE) of the HF-etched solar cell and the same solar cell before and after aging (Figure 5.8, Appendix). After accounting for measurement position variation, we saw a small increase in EQE over the region of tetracene absorption, an increase likely within the noise level of our measurement. The tetracene layer is thicker than the triplet exciton diffusion length, and charge carriers are injected near the interface where the passivation is poor, leading to little additional photocurrent from triplet excitons [2]. The following experiments will offer additional evidence for triplet exciton transfer and insight into the dynamics and mechanism.

5.2.2 Quenching of delayed photoluminescence

To investigate the mechanism, timescale, and yield of the transfer process of triplets into Si, we measured the tetracene PL decay both in the solar cells and tetracene deposited on Si wafers. The inset in Figure 5.3 a), compares the PL spectra of Si/SiO_x/tetracene and HF-Si/tetracene solar cells after exposure to air, showing the characteristic tetracene 0-0 emission peak at 535 nm with a shoulder at 580 nm due to the 0-1 transition, and a broad defect emission around 615 nm. This defect emission arises from structural defects in tetracene during the vacuum evaporation process [93, 135]. The PL spectra are the same for both the samples upon air exposure, thus the PL spectra show no evidence of additional trap states from the aging process in samples with and without the SiO_x. The PL in tetracene originates from singlet exciton emission. The PL decay shows a fast initial component due to singlet fission at short times ($<$ 1 ns, prompt PL) and a long-lived delayed PL arising from the triplet-triplet annihilation to singlet excitons at later times ($>$ 40 ns, delayed PL). The prompt PL decay is identical for the aged samples with and without the SiO_x blocking layer, showing that the singlet fission rate is not affected by the blocking layer (Figure 5.3 a). However, the delayed PL component was faster in the HF-Si/tetracene solar cell upon air exposure, which provides additional evidence for the depopulation of triplets in tetracene caused by triplet transfer into Si (Figure 5.3 b). Since triplet excitons disappear from tetracene because they are transferred into Si, triplet-triplet annihilation is reduced which in turn reduces the delayed PL intensity. The PL lifetime measurements have been reproduced with solar cell samples having a SiN blocking layer (Figure 5.9, Appendix) showing no evidence for triplet transfer, just like in the SiO_x samples. The samples with and without the blocking layer in Figure 5.3 b) and Figure 5.9 have been aged under similar conditions, the tetracene layer was exposed to air in all cases but we only see delayed PL quenching in the sample without the interlayer. We can, therefore, exclude that oxygen quenching of the triplets leads to the faster delayed PL. The samples with the SiN blocking layer and HF-Si have been measured at different spots of the solar cell (Figure 5.10, Appendix), and showed no dependence on the measurement position on

the samples. To reconfirm the results PL decay measurements were performed in tetracene deposited on Si wafers (i.e., not a full solar cell) with and without the SiO_x blocking layer, and similar results were obtained (see Figure 5.11, Appendix). This ensures that the observed PL dynamics are a characteristic of the HF-Si/tetracene interface, and that it is not influenced by the presence of other solar cell components. Together with the magnetic field-dependent photocurrent measurements, we correlate the faster decay in the delayed PL to triplet quenching to the triplet transfer process from tetracene into Si.

5.2.3 Tetracene Polymorphism

What is the mechanism of activating triplet transfer in the HF-Si/tetracene samples after aging in the air? The activation could originate from either a change in the tetracene or of the HF-Si interface or both. We deployed X-Ray diffraction (XRD) to detect changes in the tetracene morphology and X-ray Photoemission Spectroscopy (XPS) to investigate changes on the HF-Si surface.

Two different polymorphs, created by heated (TCI) or cooled (TCII) substrates can form during tetracene deposition.

The TCII polymorph has different packing with increased distance along the c-axis compared to TCI, resulting in a lower diffraction angle in XRD along the (00c) diffraction [112]. Before air exposure, the XRD spectra show the presence of both polymorphs with slightly more TCI ($2\Theta = 7.3$) compared to TCII ($2\Theta = 6.9$) as seen in Figure 5.4. However, after air exposure, the ratio reversed with more TCII compared to TCI, suggesting a change in polymorphism in tetracene. The two polymorphs have different intermolecular coupling strengths due to a difference in molecular orientations that leads to a faster singlet fission rate in TCII compared to TCI as reported by Arias et al [5]. The transition between both polymorphs is smooth (Figure 5.12, Appendix) and is not triggered when storing the samples in nitrogen for seven months (Figure 5.13, Appendix). We also observe a change in singlet fission rate, as the prompt PL decay of tetracene deposited on quartz becomes faster after air exposure

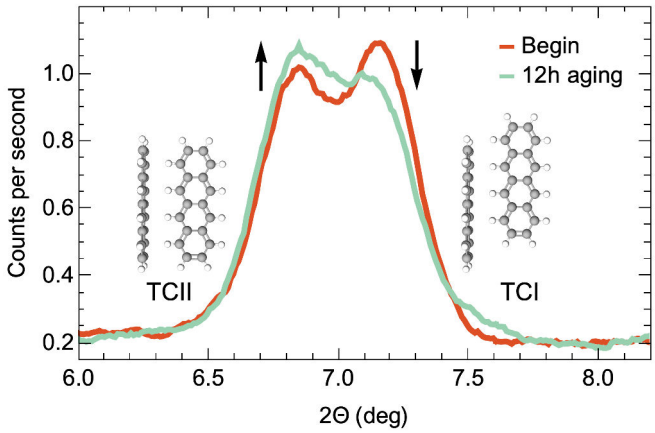

Figure 5.4: XRD of tetracene deposited on fresh HF-Si/tetracene and after 12 h of air exposure. We observe a conversion of TCI to TCII.

(Figure 5.14, Appendix). To confirm that the change responsible for triplet transfer is the aging of tetracene and not the aging of the HF-Si surface we exposed HF-Si samples to air for different amounts of time, to grow a SiO_x layer with various thicknesses. We measured XPS to confirm the growth of this SiO_x overlay by monitoring the Si-O_x peak in the Si 2p photoelectron emission narrow scan (Figure 5.15 a) and b), Appendix). On these samples, we deposited fresh tetracene and measured the PL-decay. Triplet transfer was not observed in these samples (Figure 5.15 c), Appendix) confirming that triplet transfer is not associated with the growth of a SiO_x layer, and the aging and subsequent change in the polymorphism of tetracene is related to the triplet transfer. Triplet transfer via a direct Dexter-type mechanism is dependent on the overlap between the triplet exciton wavefunction of tetracene and of the electron and hole wavefunctions at the Si surface [24]. This coupling will change depending on the distance and orientation of the tetracene molecules with respect to the Si surface. Therefore, the change in the orbital coupling in going from TCI to TCII and its effect on the triplet transfer efficiency is likely crucial and needs to be investigated further theoretically. A recent report by Niederhausen et al. that deployed near-edge X-ray absorption fine

structure (NEXAFS), XPS, and density functional theory (DFT) calculations also suggests that different orientations at the interface exist and could lead to a change in transfer efficiency [85].

5.2.4 Triplet Transfer Efficiency

To extract the triplet transfer rate and transfer efficiency we model the PL decay data considering the singlet fission process as depicted in Figure 5.5 a) [5, 95, 141]. The singlet fission process in tetracene (with rate: k_{SF}) competes with the radiative decay (k_{Rad}) through the formation of triplet pairs, which can then dissociate (k_{Diss}) to form free triplets or fuse back (k_{TT}) to create an excited singlet state. The free triplets can decay with the triplet lifetime (k_{Trip}), or regenerate the triplet pair state through triplet-triplet annihilation (k_{TTA}). TTA results in the delayed PL from tetracene and determines the triplet lifetime [10, 43, 95]. The populations of the S_1, TT and T states can be determined by solving the coupled differential equations as detailed in the Appendix. The S_1 population is plotted against the measured PL decay traces in Figure 5.3 (dotted lines) for the prompt and delayed PL. The rate constants described above were determined by solving the differential equation for HF-Si/tetracene before and after exposure to air and using a least-squares algorithm to fit the data as described in the Appendix. The rate constants obtained are in agreement with the literature as shown in Table 1, Appendix. The singlet fission time constant was determined to be 220 ± 1 ps, which is in good agreement with reported values of $\sim 75 - 200$ ps depending on the crystallinity, grain size and preparation conditions [5, 10, 93, 95, 141, 148]. The faster decay of the delayed PL can be reproduced with the kinetic model by incorporating an additional triplet transfer process to Si without changing the other rate constants. The model based on these kinetic equations reproduces the data for prompt (until 1.7 ns) and delayed PL (> 30 ns) well, but fails to describe the decay at intermediate times between prompt and delayed PL. This is most likely due to additional effects of triplet pair diffusion, which have been explained by modeling that leads to a $t^{-\frac{3}{2}}$ dependence of the PL decay [113]. Our

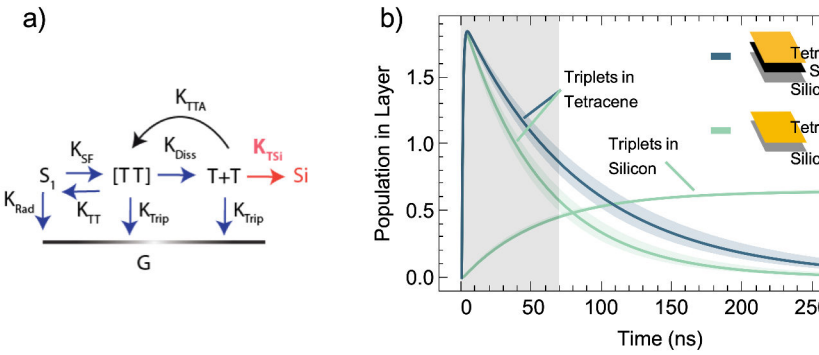

Figure 5.5: a) Schematic representation of the kinetic model used to determine the triplet transfer efficiency b) the triplet population in Si/SiO_x/tetracene (control), HF-Si/tetracene and in HF-Si after air exposure predicted from our model as a function of time. The grey area shows our experimental range of the PL decay measurements (70 ns). Transparent bands are 95 % confidence intervals of the fitting parameters.

intermediate PL decay data is also described by this function (Figure 5.16, Appendix) [113].

From the kinetic model, the triplet lifetime is 85 ± 6 ns in both samples and the triplet transfer time into Si is 169 ± 8 ns in the aged sample. Figure 5.5 b) shows how the triplet population varies with time with a faster decay of the triplet population in HF-Si due to triplet transfer into Si. The growth of the triplet population in HF-Si corresponds to 35.7 % ± 0.9 % of triplet transfer. Our model is robust against sample-to-sample variation, aging of tetracene on its own, and between wafers and solar cell (see Appendix Figure 5.9, Figure 5.10, Figure 5.11, Figure 5.14). Our findings show that efficient triplet transfer can be obtained when the percentage of TCII is increased. Thus, to achieve even higher triplet transfer yield into HF-Si, control over the morphology appears to be crucial, so that TCII becomes the predominant polymorph. This also suggests that apart from the complex HfO_xN_y interlayers used before,

we can also exploit the tetracene orientation itself for efficient triplet transfer [29].

5.3 CONCLUSION

In summary, we have shown that a change in the dominant tetracene polymorph by air exposure facilitates triplet transfer from tetracene into Si. The triplet transfer process is confirmed through magnetic field-dependent photocurrent measurements, and the timescale of triplet transfer is obtained from delayed PL decay measurements. We find that the transition from the tetracene polymorph TCI to TCII is essential for efficient triplet transfer. This suggests that the orientation (w.r.t. the surface), and the packing of the singlet fission molecule is crucial for an efficient triplet transfer process. Future research should focus on an optimal alignment of tetracene molecules by preparing a pure TCII polymorph on Si and potential combinations of both interlayers and polymorph control, which could lead to the optimal triplet transfer efficiency. This could then enable the cheap manufacturing of singlet fission-sensitized Si solar cells.

5.4 EXPERIMENTAL DETAILS

Solar cells

The solar cells are Interdigitated Back Contact (IBC) silicon solar cells with a silicon pyramid antireflection layer and a $\sim 80\,\text{nm}$ SiN passivation and antireflection layer. We cut the $4\,\text{cm} \times 4\,\text{cm}$ solar cells in three stripes with a laser cutter. We use a wire bonder to contact the back-side contacts to contact pads for the photocurrent measurements.

Silicon Wafers

Silicon Wafers were purchased from Siegert Wafer GmbH. We used <111> FZ-silicon, n-doped (Ph) with a resistivity of $1-5\,\Omega\,\mathrm{cm}$, Double side polished with a thickness of 0.28 mm. We dice the wafers using a laser cutter.

HF etching of solar cells

We dripped concentrated hydrofluoric acid (HF) solution (40 %, Sigma-Aldrich, as received) onto the top surface of the silicon solar cell with a pipette. In this way the HF solution does not contact the metallic back contacts. After 10 min of etching the wettability decreases dramatically, meaning that at this point we have etched away the SiN which has a lower contact angle than the bare Si surface. We then removed any of the remaining HF solution from the surface by dipping the samples sequentially twice in deionized water baths. Immediately afterwards, the sample was transferred into a nitrogen-filled glovebox.

Tetracene deposition

We deposited 200 nm of tetracene onto the silicon solar cells, and either 35 nm or 200 nm onto the bare silicon samples. The evaporation was done inside a thermal evaporator (Angstrom Engineering Inc.), at a base pressure below $7\cdot10^{-7}$ mbar. Tetracene was purchased from Sigma-aldrich (99.99 % purity) and used as is. The deposition rate was $1\,\frac{\text{Å}}{\text{s}}$ in all cases. Encapsulation was also done inside the nitrogen-filled glove box, using two glass slides, a rubber gasket and silicone glue. None of the samples were exposed to UV light during storage and measurement.

Magnetic-field dependent photocurrent measurements

We measured the magnetic-field dependent photocurrent using a home-built setup. The magnetic field is applied by an electromagnet, made up by two Helmholtz coils and calibrated using a Hall effect sensor. The

magnetic field is applied by sending a current of up to 5 A of current through the coils, resulting in a magnetic field of up to 0.35 T. The field is oriented parallel to the sample surface. The excitation source is a 520 nm diode laser, installed in a Thorlabs temperature-controlled laser housing. The cw laser power is around 10 mW with a laser spot size of approximately 1 mm. The photocurrent is measured with a Keithly 2636A source-measure unit. After each measurement at a certain magnetic field we perform a reference measurement at zero magnetic field. For the self-passivation measurements we added a 100 W xenon lamp with a 550 nm longpass filter, to only excite the silicon substrate.

Photoluminescence studies

Photoluminescence (PL) spectra and decay kinetics were monitored in Lifespec-ps (Edinburgh Instruments) upon 404 nm laser pulse (pulse width ~ 100 ps) excitation with a repetition rate of 200 kHz. The tetracene-deposited substrates were encapsulated inside a custom-made sample holder inside a glovebox prior to the measurement. Afterwards, the samples were exposed to air and encapsulated again inside the glovebox to investigate the effect of air exposure on PL decay.

X-Ray diffraction

XRD was measured on a Bruker D2 Phaser using a Cu Tube with 1.54 Å at 10 mA and 30 kV as a source. We used a Lynxeye detector in 2Theta mode with a scan speed of 420 s per measurement. Each 7 min we measure the diffraction spectra once. The sample was rotating at 10 per min and kept inside the instrument during the whole measurement. We use a moving average over 21 points to smooth the diffraction curve. After tetracene deposition the devices were stored in a nitrogen-filled glovebox before the XRD measurement. The storage time inside the glovebox was 1 month for the sample in the main text and 7 months in the sample described in the Appendix.

X-Ray Photoelectron spectroscopy

XPS measurements were performed with a JEOL JPS-9200 photoelectron spectrometer, using a 12 kV and 20 mA monochromatic Al Kα source. The analyzer pass energy was 10 eV, and the take-off angle between sample and detector was set at 10°. Data was analyzed using the CasaXPS program, version 2.3.18PR1.0. To measure the samples, the silicon surfaces with tetracene layer were transferred in an air-tight container from a glovebox $O_2 < 0.01$ ppm, $H_2O < 0.01$ ppm to the XPS, to minimize air exposure during transfer. In the XPS, a first dummy measurement taking ~100 min was performed, to heat up the sample stage. This, in combination with the high vacuum in the measurement chamber $10^{-5} - 10^{-6}$ mbar, led to the sublimation of tetracene from the sample, leaving the bare silicon surface behind. The level of silicon surface oxidation was then assessed by performing narrow scans on the silicon 2p peak. The relative surface area of the Si 2p peak at ~ 103 eV was taken as a measure for surface oxidation.

5.5 APPENDIX

ADDITIONAL MAGNETIC-FIELD DEPENDENT PHOTOCURRENT REFERENCE MEASUREMENTS

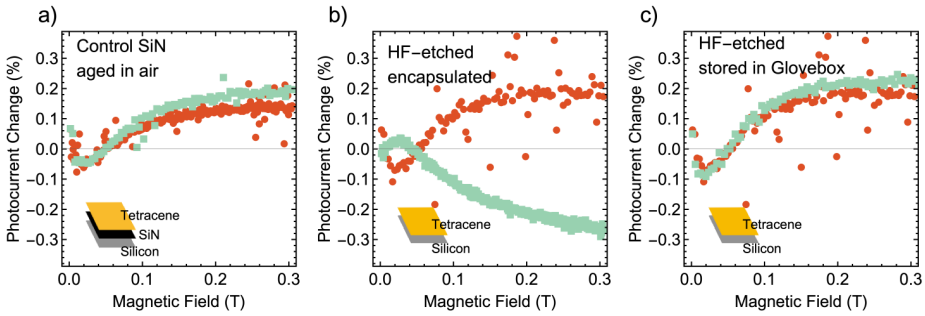

Figure 5.6: . Magnetic field-dependent photocurrent in a) Si/SiN/tetracene solar cell before (green curve) and after aging (red curve) in air with no change in triplet transfer behavior. b) Encapsulated HF-Si/tetracene silicon solar cell stored in air for six weeks. The photocurrent change flips from singlet to triplet curve, and c) HF-Si/tetracene solar cell stored under nitrogen atmosphere in the glovebox for six weeks without changes to the triplet transfer.

ABSENCE OF SELF PASSIVATION EFFECT

To investigate whether the self-passivation of additional charge carriers in silicon can lead to an overestimation of the magnetic field effect, we add an additional red light with energy below the tetracene bandgap so that the light is only absorbed in the silicon layer. The change in photocurrent with magnetic field can be written as $\Delta I(B) = (I(B) - I(B = 0))/I(B)$. If we add different light sources, each light source will add current that can also be dependent on the magnetic field. In our experiment we added red light (leading to current $I_{Red}(B)$) to the green laser (current $I_{Green}(B)$). The change in photocurrent then becomes

$$\begin{aligned}\Delta I(B) = {} & I^{Tc}_{Red}(B) + I^{Si}_{Red}(B) + I^{Tc}_{Green}(B) + I^{Si}_{Green}(B) \\ & - I^{Tc}_{Red}(B = 0) - I^{Si}_{Red}(0) - I^{Tc}_{Green}(0) - I^{Si}_{Green}(0)\end{aligned}$$

Since tetracene does not absorb in the red, we set $I^{Tc}_{Red}(B) = 0$. The current generated in silicon directly does not depend on the magnetic field, leading to $I^{Si}(B) = I^{Si}(0)$, leaving us with:

$$\Delta I(B) = \frac{I^{Tc}_{Green}(B) - I^{Tc}_{Green}(0)}{I_{Green}(0) + I_{Red}(0)}$$

We measure the current from only the red light at zero field and then correct the magnetic field curve with the formula above.

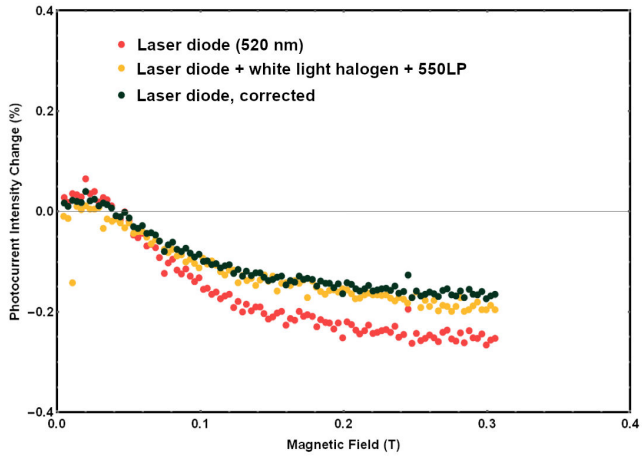

Figure 5.7: Change in photocurrent of HF-Si/tetracene solar cell under magnetic field with different light sources. Illumination with the green laser (red curve), illumination with green laser and red light (yellow), and correcting the red curve with the formula described below. If accounted for the additional charge carriers, both curves are on top of each other and we can conclude that there is a negligible effect of self passivation from the additional charge carriers in silicon.

EXTERNAL QUANTUM EFFICIENCY

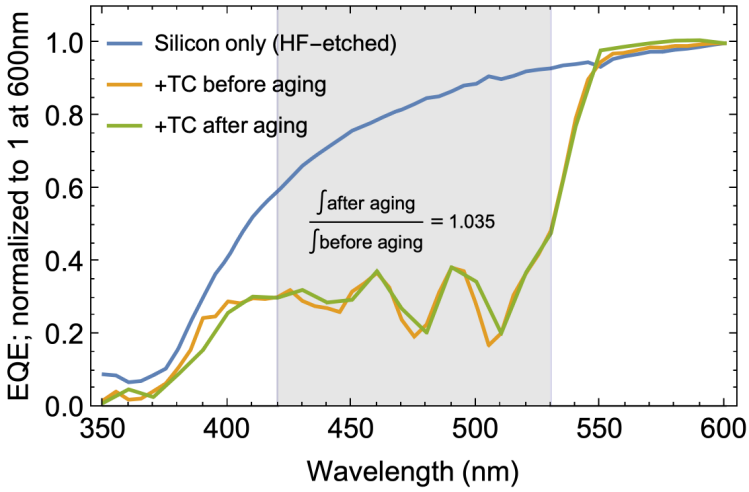

Figure 5.8: Normalized EQE of the silicon only, silicon/tetracene and silicon/tetracene (aged) solar cells in the region of tetracene absorption. These cells correspond to the magnetic-field dependent measurements presented in Figure 5.2 of the main text. The EQE is normalized to 1 at 600 nm to account for variability between measurement positions. The integral over the shaded area of 420 nm to 530 nm increases by 3.5 % upon aging, a small number most likely within the measurement error. The poor surface passivation and therefore lack of charge collection at the interface, and the transport of triplet excitons to the interfaces are the most likely reasons for this small absolute gain in EQE.

SOLAR CELL WITH SIN LAYER PHOTOLUMINESCENCE DECAY AND MODELING

We model the PL decay from the solar cell with a SiN interlayer. The data with the fit is shown in 5.9 c) with the resulting triplet densities in Figure 5.9 d). From the fit we observe a triplet transfer efficiency of 34.5 % ± 0.01 %, comparable to the 35.7 % in the main text with the SiO_x interlayer. The error is dominated by the fitting error of the triplet transfer rate, which is small. The kinetic parameters extracted from the model for Si/SiN/tetracene (aged) are $k_{sf} = (258.6 \pm 0.9\,ps)^{-1}$; $k_{rad} = (12.5\,ns)^{-1}$ (kept constant); $k_{TT} = (10360 \pm 750\,ps)^{-1}$; $k_{Diss} = (1337 \pm 137\,ps)^{-1}$;$k_{TTA} = (9.6 \pm 0.9) \cdot 10^{-11} cm^3 s^{-1}$; $k_{Trip} = (78 \pm 5\,ns)^{-1}$. For HF-Si/tetracene (aged) a triplet transfer rate of $k_{T\rightarrow Si} = (171 \pm 11\,ns)^{-1}$ and $k_{sf} = (217.2 \pm 0.5\,ps)^{-1}$ was fitted.

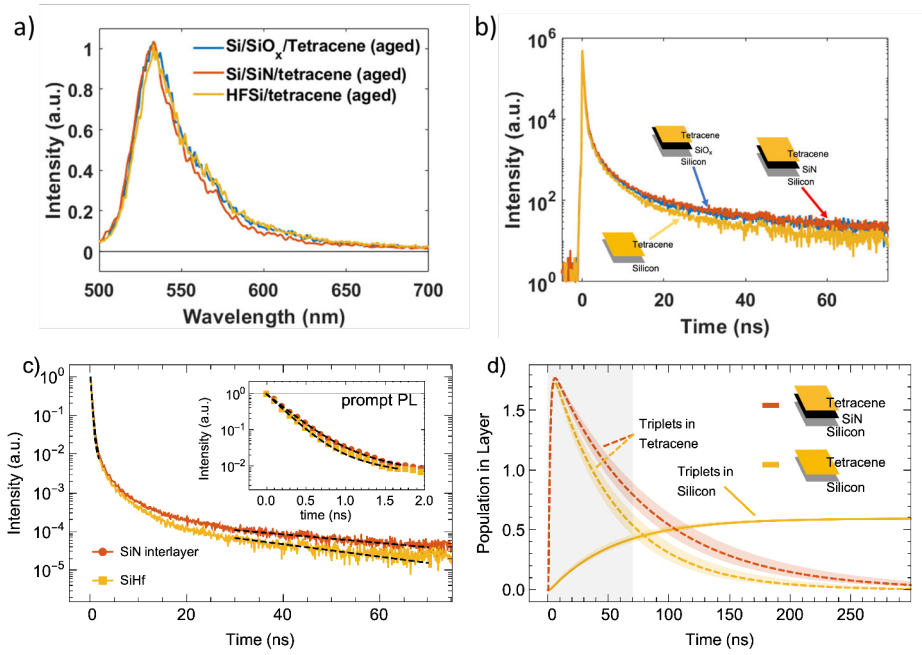

Figure 5.9: a) PL spectra of tetracene show the absence of degradation and additional trap states, and b) decay traces for tetracene deposited on Si/SiO_x, Si/SiN and HF-Si solar cells, showing no difference between slope of the long-time decay for the SiN and SiO_x blocking layers and triplet quenching in fresh HF-Si. c) kinetic modeling of the SiN vs the SiHF (aged) solar cell to investigate the influence of the interlayer on transfer efficiency. d) Triplet population in tetracene and silicon derived from the kinetic modeling shown in Figure 5.9 c). The bands around the model in Figure 5.9 d) are 95% confidence intervals.

SOLAR CELL PHOTOLUMINESCENCE IN DIFFERENT SPOTS

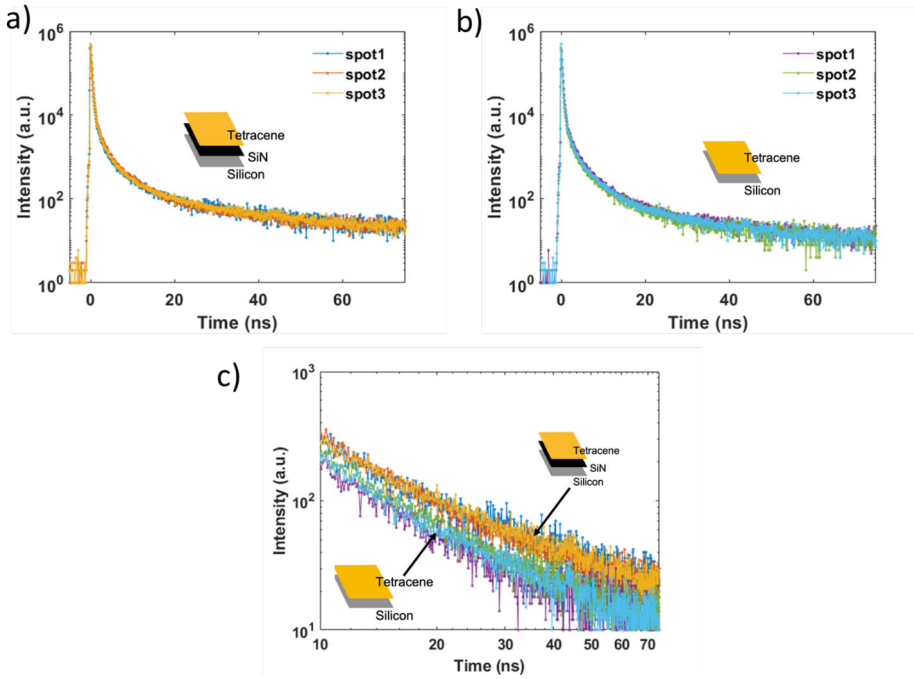

Figure 5.10: PL decay traces for a) Si/SiN and b) HF-Si solar cells sensitized with tetracene excited on different spots on the solar cell surface. c) Comparison of decay traces in a) and b) together to show the reproducibility of the data in different spots and measurements. We performed the kinetic modeling described on all nine combinations of reference (SiN) and quenching (HF-Si) samples and get a mean efficiency of 27.8% with a standard error of the mean of 2.0% and a standard deviation of 5.8% which corresponds to the sample-to-sample variation.

WAFER PHOTOLUMINESCENCE DECAY AND MODELING

We also fabricated silicon wafers, deposited tetracene and aged them. The PL spectrum (Figure 5.11 a)) shows some difference in the defect emission around 620 nm upon exposure to air, contrary to the solar cells samples. The decay dynamics show a similar behavior as the solar cell samples. The initial singlet decay becomes equally faster upon air exposure in both Si/SiO_x and HF-Si, implying a faster SF rate due to the increased concentration of TCII.

We applied the same kinetic model for tetracene on silicon *wafers* as for the solar cell samples and the outputs are shown as dotted black lines in Figure 5.11 c), together with the PL decay data. The efficiency of triplet transfer is 48.3 % ± 1.8 %, higher compared to the solar cell transfer efficiencies. The kinetic parameters extracted from the model for Si/SiO_x/tetracene (aged) are $k_{sf} = (235 \pm 1\,ps)^{-1}$; $k_{rad} = (12.5\,ns)^{-1}$ (kept constant); $k_{TT} = (3407 \pm 158\,ps)^{-1}$; $k_{Diss} = (655 \pm 24\,ps)^{-1}$; $k_{T}TA = (15.9 \pm 0.7) \cdot 10^{-11} cm^3 s^{-1}$; $k_{T}rip = (141 \pm 8.7\,ns)^{-1}$. For HF-Si/tetracene (aged) a triplet transfer rate of $k_{T\rightarrow Si} = (165.1 \pm 4.4\,ns)^{-1}$ and $k_{s}f = (226.8 \pm 0.4\,ps)^{-1}$ was fitted. The kinetic parameters are slightly different for these tetracene samples prepared on Si wafers which can be due to different sample preparation conditions and batch-to-batch variability.

To quantify the error introduced by different reference samples we use a fresh, not aged sample as a reference and perform the same model as before, seen in Figure 5.11 e) and f). The triplet transfer efficiency with this combination is 58.7 % ± 3 %, around 10 % higher than with the aged sample as a reference. This apparent 10 % higher transfer efficiency is the effect of aging of tetracene. The kinetic parameters extracted from the model for Si/SiO_x/tetracene (aged) are $k_{s}f = (255 \pm 1\,ps)^{-1}$; $k_{rad} = (12.5\,ns)^{-1}$ (kept constant); $k_{TT} = (3109 \pm 137\,ps)^{-1}$; $k_{Diss} = (724 \pm 27\,ps)^{-1}$; $k_{TTA} = (10.8 \pm 0.5) \cdot 10^{-11} cm^3 s^{-1}$; $k_{Trip} = (213 \pm 18\,ns)^{-1}$. For HF-Si/tetracene (aged) a triplet transfer rate of $k_{T\rightarrow Si} = (164.8 \pm 5.5\,ns)^{-1}$and $k_{sf} = (219.9 \pm 0.5\,ps)^{-1}$ was fitted.

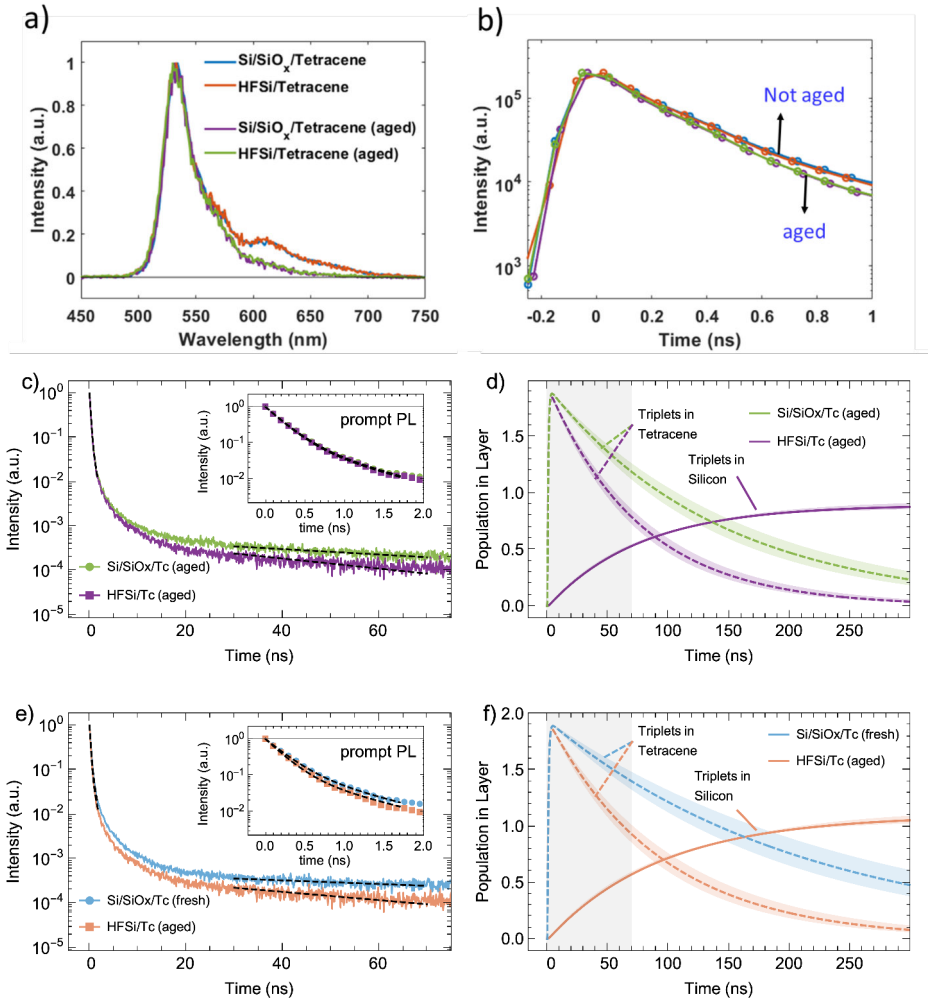

Figure 5.11: a) PL spectra, b) prompt, and c) delayed PL for tetracene deposited on Si/SiO$_x$ and HF-Si *wafers* (thus not solar cells as in the main text) with and without air exposure. The inset in c) shows the prompt PL decay. d) The triplet yield as a function of time as predicted from the model. The bands around the model are 95% confidence intervals. Panels e) and f) show kinetic modeling with a fresh Si/SiO$_x$/tetracene sample as reference sample, to quantify the influence of the aging of tetracene on top of the reference sample on the triplet efficiency of our model. The inset shows prompt PL and the different fit due the free fit parameter k_{SF}.

X-RAY DIFFRACTION MEASUREMENT OVER TIME

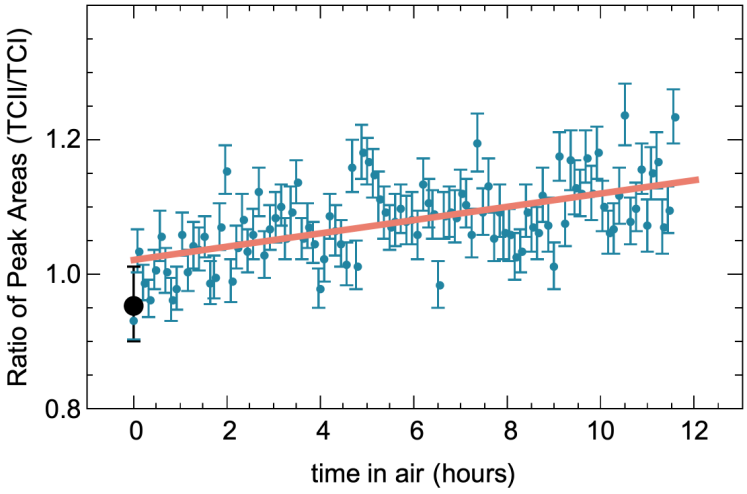

Figure 5.12: Ratio of peak areas of TCII/TCI determined from a fit of two normal functions to the XRD data, with a fixed position for TCI (7.2°) and TCII (6.8°) and free fit parameters of peak width and peak height. We observe a smooth transition between the polymorphs. The data in the main text (Figure 4) are the blue datapoints for 0 h and 12 h. In black is a measurement of a tetracene film on silicon of the same batch but stored in the glovebox for seven months (data in Figure 5.13).

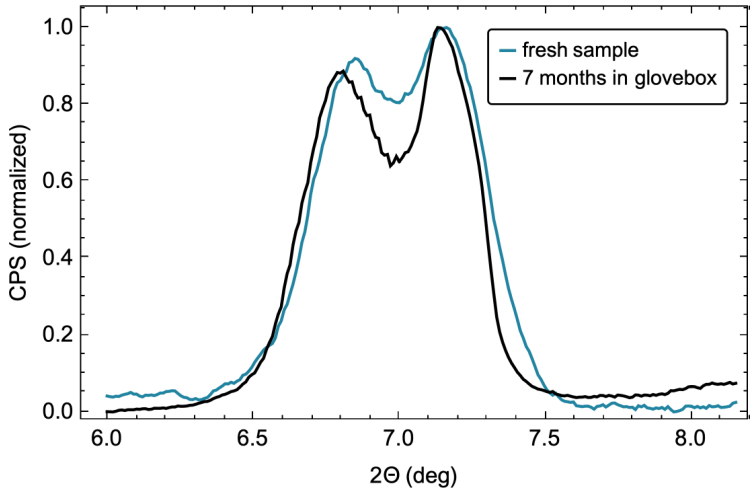

Figure 5.13: XRD measurement of tetracene films directly after removing them from the glovebox. Black when stored in glovebox for one month (data also in main text), blue when stored in the glovebox for seven months. We conclude that storage in nitrogen does not lead to a polymorphism change. Data is normalized to be between 0 and 1 and smoothed with a moving average function over 21 data points.

TETRACENE PHOTOLUMINESCENCE AGING ON QUARTZ

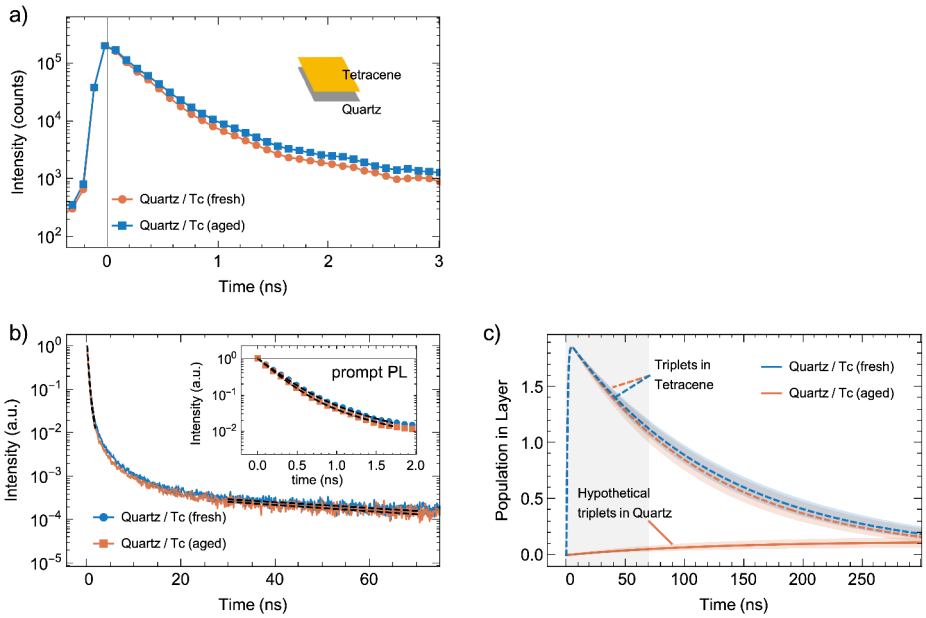

Figure 5.14: a) Prompt and b) delayed PL of tetracene deposited on quartz. The change in the initial fast decay after air exposure can be attributed to an interchange of TCI to TCII. The black lines represent the outputs from the kinetic model using the fresh tetracene sample as a reference and the aged tetracene sample as the quenched sample. We calculate this to quantify the influence of degradation of tetracene alone on our kinetic modeling. The triplet transfer efficiency obtained is 6.5 % $\pm$ 2.4 %, which means that the effect of tetracene aging alone on our model is much smaller than the transfer efficiency observed in the samples with HF-Si and aged tetracene. Panel c) shows the triplet populations as would be expected if the samples were on deposited on silicon. The bands around the model are 95 % confidence intervals.

XPS MEASUREMENT ON HF-SI AND CHANGE OVER TIME

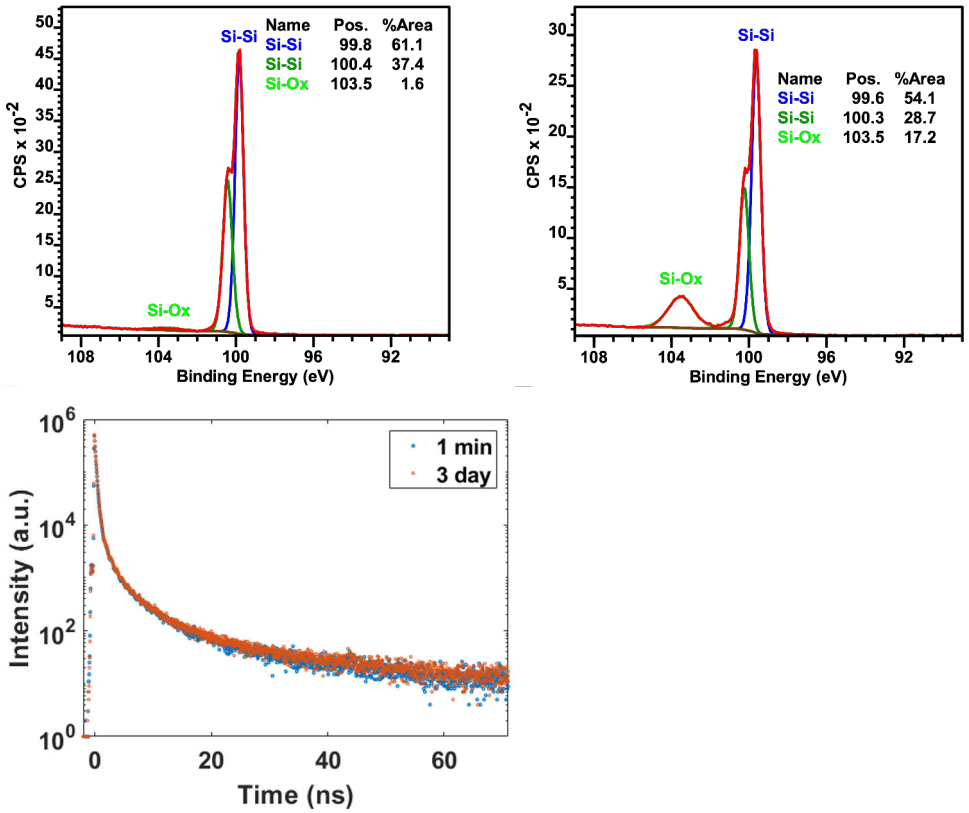

Figure 5.15: Si 2p XPS data of HF-Si sample exposed in air for a) 1 min, and b) 3 days. The difference shows the growth of SiO_x upon longer exposure. Tetracene was deposited on these pre-exposed HF-Si substrates, and the PL lifetime of tetracene in panel c) is unchanged, suggesting exposure of HF-Si to air alone does not lead to triplet transfer.

MODELING OF INTERMEDIATE PHOTOLUMINESCENCE DECAY

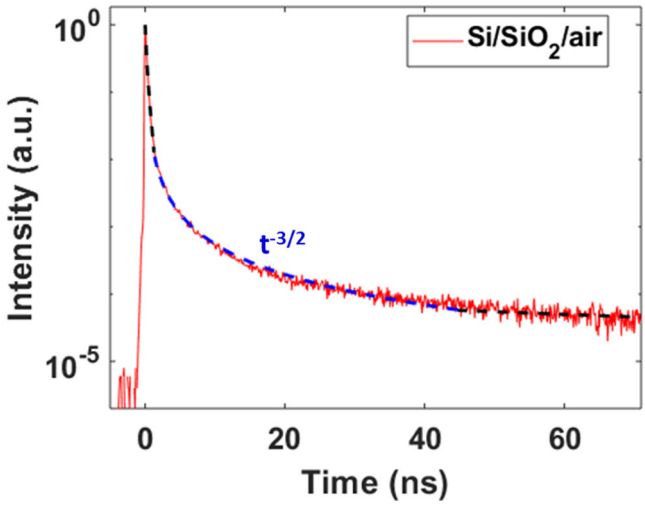

Figure 5.16: The kinetic model based on the solution of coupled differential equations reproduces the data for prompt and delayed PL (black dotted line) of tetracene deposited on Si/SiO_x. The intermediate-time region of the PL decay curve is dominated by diffusion of the triplet pair states, which follows a $t^{-\frac{3}{2}}$ dependence [113]. Here the $t^{-\frac{3}{2}}$ term was added manually to show the qualitative match with the data.

KINETIC MODELING OF TRIPLET QUENCHING

Differential equations

We set up the following set of coupled differential equations for all species present in an excited tetracene crystal *with* SiO_2interlayer:

$$\begin{aligned}
\frac{dS(t)}{dt} &= -(k_{SF} + k_{Rad})\,S(t) + k_{TT}TT(t) \\
\frac{dTT(t)}{dt} &= k_{SF}S(t) - k_{TT}TT(t) - k_{Diss}TT(t) \\
&\qquad + k_{TTA}T(t)^2 - k_{Trip}TT(t) \\
\frac{dT(t)}{dt} &= 2k_{Diss}TT(t) - 2k_{TTA}T(t)^2 - k_{Trip}T(t) \\
\frac{dG(t)}{dt} &= k_{Rad}S(t) + k_{Trip}TT(t) + k_{Trip}T(t)
\end{aligned}$$

The additional quenching in the samples *without* SiO_2 interlayer is modeled by an additional quenching term (**bold**) on the triplet density T:

$$\begin{aligned}
\frac{dS(t)}{dt} &= -(k_{SF} + k_{Rad})\,S(t) + k_{TT}TT(t) \\
\frac{dTT(t)}{dt} &= k_{SF}S(t) - k_{TT}TT(t) - k_{Diss}TT(t) \\
&\qquad + k_{TTA}T(t)^2 - k_{Trip}TT(t) \\
\frac{dT(t)}{dt} &= 2k_{Diss}TT(t) - 2k_{TTA}T(t)^2 - k_{Trip}T(t) - \mathbf{k_{T\to Si}T(t)} \\
\mathbf{\frac{dT_{Si}(t)}{dt}} &= \mathbf{k_{T\to Si}T(t)} \\
\frac{dG(t)}{dt} &= k_{Rad}S(t) + k_{Trip}TT(t) + k_{Trip}T(t)
\end{aligned}$$

The singlet (S_1) produces a triplet pair (TT) state through singlet fission (k_{SF}), which then dissociates (k_{Diss}) into free triplets (T). Both singlet, triplet and triplet pair can recombine to the ground state (G).

The radiative decay of the S_1 state has a lifetime of 12.5 ns (taken from literature, Table 1). The TT state decays back to a S_1 state with the rate k_{TT}. The free triplets can regenerate the TT state through triplet-triplet annihilation (k_{TTA}). The triplet state or triplet pair state decay non-radiatively (k_{Trip}) to the ground state. Upon air exposure, triplet transfer to Si also diminishes the triplet population through triplet transfer to Si $k_{T\rightarrow Si}$.

Fitting procedure of differential equation to PL decay

We are solving the differential equations above using ParametricNDSolve and NonlinearModelFit functions in MATHEMATICA 12.1. The initial boundary conditions are $S(t=0) = 2 \cdot 10^{16}\,cm^{-3}$ (the laser power density), $T(t=0) = 0$, and $TT(t=0) = 0$. First, we fit the reference PL-decay to the prompt PL data between 0 ns and 1.7 ns and then delayed PL data between 30 ns to 70 ns to the singlet population of the differential equations above (the PL is proportional to the singlet population for excitonic PL). After 70 ns the afterpulsing of our single photon counter starts to affect the measurement. All parameters except for k_{rad} are free, with literature values used as starting values. We use weights of $1/N_i$ for the fit (N_i is the number of counts at each time t_i) to account for the Poisson counting error. We do not fit the intermediate part of the decay (1.7 ns to 30 ns) where the triplet diffusion dominates (see Figure 5.16). After fitting the reference sample we fit the data from the quenching sample to estimate the transfer efficiency. We use the reference rate constants and add a quenching term to the triplet state population. Since the tetracene is aged in both reference and quenching data the other rates are assumed to be constant, except for k_{sf} which can vary slightly upon aging as seen from the SiN interlayer data shown in Figure 5.11 e). We calculate the 95% confidence bands for the triplet population by varying each rate by the confidence interval, which assumes that the parameters have negligible covariances. The triplet transfer efficiency is calculated from the triplet population in silicon at long times after saturation (> 500 ns) divided by the maximum of the triplet population in tetracene upon excitation.

	Solar cell sample exposed to air		Literature			
	Si/SiO_2	HF-Si	fs-TA on single cryst. [5]	fs-TA polycryst. [148]	PL decay polycryst. [141]	Reference [95]
k_{SF}	Fitted $(220 \pm 1\,ps)^{-1}$	Fitted $(212 \pm 1\,ps)^{-1}$	$(124\,ps)^{-1}$	$(120\,ps)^{-1}$	$(90\,ps)^{-1}$	$(180\,ps)^{-1}$
k_{Rad}	Set to $(12.5\,ns)^{-1}$	Set to $(12.\,ns)^{-1}$	$(524ps)^{-1}$	$(12.5ns)^{-1}$	$(12.5ns)^{-1}$	$(12.5ns)^{-1}$
k_{TT}	Fitted $(6303 \pm 304\,ps)^{-1}$	Set to $(6303\,ps)^{-1}$	$(360\,ps)^{-1}$	$(1000\,ps)^{-1}$	$(150\,ps)^{-1}$	$(100\,ns)^{-1}$ [1]
k_{Diss}	Fitted $(810 \pm 36\,ps)^{-1}$	Set to $(810\,ps)^{-1}$	$(439\,ps)^{-1}$	$(500\,ps)^{-1}$	$(600\,ps)^{-1}$	–
k_{TTA}	Fitted $(9.2 \pm 0.7) \cdot 10^{-11} \frac{cm^3}{s}$	Set to $9.2 \cdot 10^{-11} \frac{cm^3}{s}$	0	$1.7 \cdot 10^{-11} \frac{cm^3}{s}$	0	
k_{Trip}	Fitted $(85 \pm 6\,ns)^{-1}$	Set to $(85\,ns)^{-1}$	$(21.59\,ns)^{-1}$	$(62.5\,\mu s)^{-1}$	$(20\,ns)^{-1}$	$(200\,ns)^{-1}$
$k_{T \to Si}$	Set to 0	Fitted $(169 \pm 8\,ns)^{-1}$	-	-	-	-

Table 5.1: Comparison of rate constants determined from the above model with literature values for tetracene singlet fission process. TA = transient absorption; PL = photoluminescence